ACS APPLIED MATERIALS & INTERFACES

www.acsami.org

Research Article

Nanosheets and Hydrogels Formed by 2 nm Metal–Organic Cages with Electrostatic Interaction

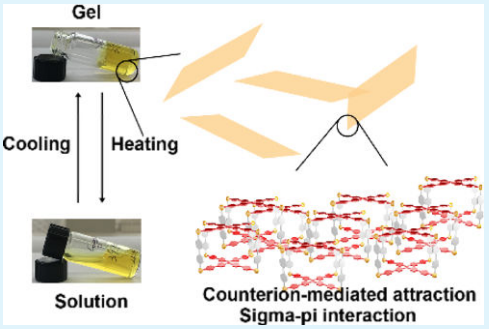
Yuqing Yang, Pavel Rehak, Ting-Zheng Xie, Yi Feng, Xinyu Sun, Jiahui Chen, Hui Li,* Petr Král,* and Tianbo Liu*

Cite This: *ACS Appl. Mater. Interfaces* 2020, 12, 56310–56318

Read Online

ACCESS | Metrics & More | Article Recommendations | Supporting Information

ABSTRACT: We report the mechanism of hydrogel formation in dilute aqueous solutions (>15 mg/mL) by 2 nm metal–organic cages (MOCs). Experiments and all-atom simulations confirm that with the addition of small electrolytes, the MOCs self-assemble into 2D nanosheets via counterion-mediated attraction because of their unique molecular structure and charge distribution as well as $\sigma-\pi$ interactions. The stiff nanosheets are difficult to bend into 3-D hollow, spherical blackberry type structures, as observed in many other macroion systems. Instead, they stay in solution and their very large excluded volumes lead to gelation at low (~1.5 wt %) MOC concentrations, with additional help from hydrophobic and partial $\pi-\pi$ interactions similar to the gelation of graphene oxides.



KEYWORDS: *supramolecular hydrogel, nanosheet, metal–organic cage, electrostatic interaction, $\sigma-\pi$ interaction*

Downloaded via UNIV OF ILLINOIS CHICAGO on January 19, 2021 at 19:24:31 (UTC).
See https://pubs.acs.org/sharingguidelines for options on how to legitimately share published articles.

INTRODUCTION

Nanosheets with atomic or molecular thickness and large surface area have many promising applications.[1] The molecular-based bottom-up nanosheets gain much attention because of their structural diversity, while the growth mechanism is still actively debated.[2−5]

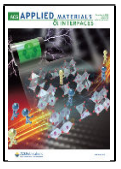
Hydrogels have been widely applied in drug delivery,[6] sensing,[7] tissue engineering,[8] cosmetic industry,[9] food packaging,[10] petroleum industry,[11] and so forth. The water environment makes the hydrophobic interaction, hydrogen bonding, and electrostatic interaction exhibit unique features. An internal network structure can be obtained through chemical bonding or physical interactions. Among them, supramolecular hydrogels have attracted enormous attention because of their self-healing[12,13] and stimuli-responsive properties[13−17] (sensitive to pH, chemical environment, or temperature), provided by the dynamic and reversible nature of noncovalent interactions. Many interactions including metal-coordination,[18,19] hydrogen bond,[19,20] $\pi-\pi$ interactions,[21−25] hydrophobic interactions,[21,23,24] host–guest interactions,[14,16,17,19,26,27] or polymer chain entanglement[28] are involved in the gel formation. Meanwhile, electrostatic crosslinking has been found to play a role in various polyelectrolyte hydrogel systems.[29−32] The electrostatic interactions, induced by cationic and anionic polyelectrolytes, create electrostatic crosslinking to facilitate the hydrogel formation. However, the gelation of low-molecular-weight structures based on electrostatic interactions has been rarely explored. To the best of our knowledge, there are very few examples of supramolecular gels based on electrostatic interaction and $\sigma-\pi$ interaction.[33]

Metal–ligand coordination-driven self-assembly is well established for constructing supramolecular structures with great control over designing 2D and 3D architectures,[34−45] such as metal–organic cycles (metallacycles) and metal–organic cages (metallacages, MOCs). Recently, supramolecular gels based on MOCs have been observed with building structures such as rodlike structures,[22] fibrous structures,[14,18,27,46] and nanoparticles[15] at critical gelation concentration (CGC) ranging from 5[21] to >100 mg/mL.[14]

The key issue for the gelation of small molecules is their self-assembly into anisotropic and open supramolecular structures, in which the electrostatic interaction is not the common driving force. The large excluded volume of these open structures would increase the lifetime of the interparticle bond to make them able to sustain stress, surviving for the time longer than the experimental probe characteristic time,[47−49] thus contributing the transition from solution to gel.

To understand such gelation processes with the goal to manipulate the sol–gel transitions, it is critical to identify the driving forces of the supramolecular structure formation.

Received: September 12, 2020
Accepted: November 16, 2020
Published: December 3, 2020



© 2020 American Chemical Society

https://dx.doi.org/10.1021/acsami.0c16366
ACS Appl. Mater. Interfaces 2020, 12, 56310–56318

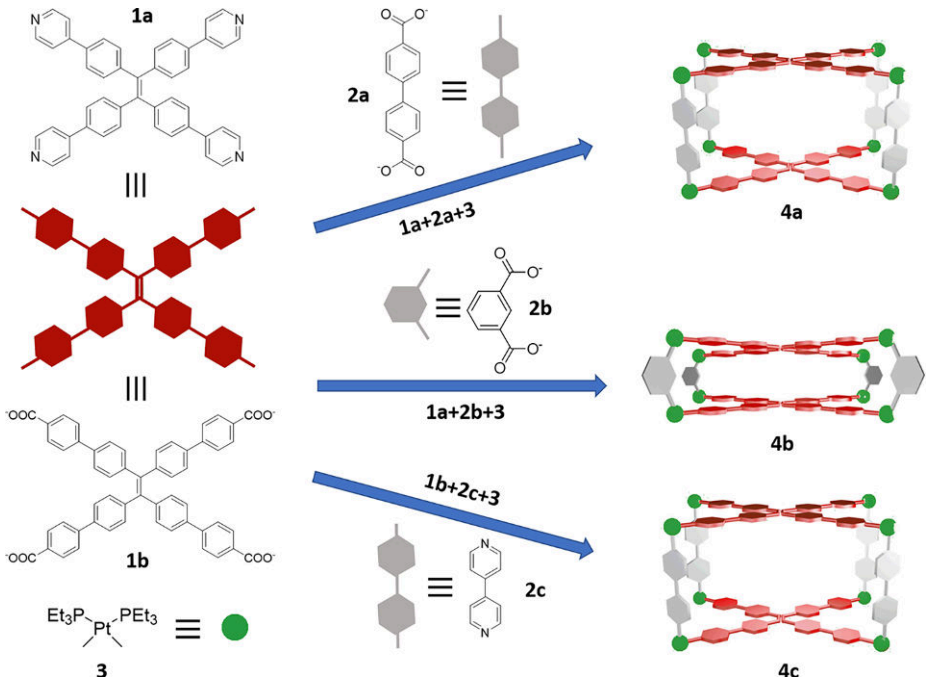


Figure 1. Self-assembly of the MOCs **4a**−**4c** using ligands **1a**, **1b**, **2a**, **2b**, and metal ion **3** with NO_3^- as counterions.

Supramolecular gel from MOCs has been reported based on dynamic coordination bonds,[21] charge-assisted H-bonds,[50] or host−guest interactions[27] with organic[14,21,23,27] or mixed solvents.[15,18,22,23,46] It is known that nanoscale charged molecules (macroions, including MOCs) can attract each other via counterion-mediated attraction. Simulation results also confirm that the formation of 2D nanosheets is a common option, which often spontaneously bend and form hollow, spherical, single-layered blackberry-type structures.[51] Because such closed supramolecular structures do not possess large excluded volumes, gelation usually does not occur. Therefore, to seek for electrostatic interaction-based hydrogels, a viable approach is to choose macroions which can attract each other but restrain their assembly to open structures with the help of additional forces.[52] Herein, we demonstrate the gelation of a 2 nm cuboid MOC (**4a**, Figure 1) based mainly on electrostatic and $\sigma-\pi$ interactions in an aqueous solution.

RESULTS AND DISCUSSION

Through the self-assembly of TPE-based ligands **1a** or **1b**, the dicarboxylate ligand **2a** or **2b**, and cis-Pt$(PEt_3)_2$ **3**, the MOCs **4a**, **4b**, and **4c**, respectively, were prepared according to previously reported methods.[53,54]

At low concentrations, most **4a** exist as discrete macrocations in an aqueous solution. From static light scattering (SLS) measurements, the scattered intensity from a 15.0 mg/mL solution of **4a** was recorded as only 204 kcps (50 times higher than that from the solvent). At the same time, dynamic light scattering (DLS) result (Figure S5) illustrated that >99% cages are single cages with a hydrodynamic radius of R_h = 1.5 nm. In this solution, the single cages coexist with a tiny portion of aggregates with average $R_h \sim 21.4$ nm. The SAXS study (Figure S6) also showed that the basic unit is MOC with a radius of gyration of R_g = 1.2 nm (indirect Fourier transformation). Higher cage concentrations will strengthen the counterion association process and promote the formation of small aggregates, which is shown by the SLS study (scattered intensity at 1583 kcps for the 20 mg/mL solution, 100 times higher than that for water). However, these solutions do not undergo obvious macrophase separation, and no precipitation is observed after 1 month. Increasing the temperature can accelerate the dissolution process.

For some macroions (e.g., MOC $Pd_{12}L_{24}$[55,56] and some polyoxometalates[57]), the addition of extra electrolytes leads to a stronger macroion−counterion association and consequently the formation of blackberry-type self-assembled structures (a microphase separation based on counterion-mediated attraction) or even precipitates (macrophase separation). The process depends on the amount and the valence of the counterions. Here, at low cage concentrations (e.g., 10.0 mg/mL), adding appropriate amount of $NaNO_3$ to the aqueous solution of **4a** does not affect the intactness of individual cages (Figure S7) but only promotes NO_3^- ions associated onto **4a**, gradually leading to a stronger cage−cage attraction. The SLS study showed an increment in scattered intensity, and DLS measurements confirmed that large aggregates were formed. At the same time, the solution became more and more viscous. Precipitation was observed when >40 equiv of $NaNO_3$ was added.

Interestingly, the addition of $NaNO_3$ into concentrated aqueous solutions of **4a** (≥15.0 mg/mL) leads to hydrogel formation. When 8 molar equiv of $NaNO_3$ was added into 20.0 mg/mL **4a** solution, the solution turned into gel within seconds. This transparent gel has the same yellow color as the solution (Figure 2). Heating the gel at 90 °C leads to a transparent and viscous solution and the gel phase can be recovered after bringing the solution back to room temperature. This reversible sol−gel transition suggests that the gel formed from **4a** in water is a physical gel based on noncovalent interactions. Because no strong NMR signal can be obtained from the cages in D_2O,[54] the gel was dried and redissolved in CD_3CN, which leads to very similar ^1H NMR spectra (Figure S10), further confirming that the cages are stable during the process and the gelation is not based on a chemical reaction.

https://dx.doi.org/10.1021/acsami.0c16366
ACS Appl. Mater. Interfaces 2020, 12, 56310−56318

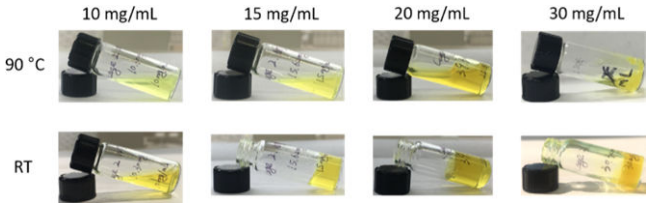


Figure 2. Sol−gel process of **4a** in aqueous solutions (10−30 mg/mL) at 90 °C and room temperature with the addition of 8 equiv of $NaNO_3$. CMC is determined as 15 mg/mL.

With 8 equiv of $NaNO_3$, CGC was ∼15 mg/mL: below the CGC, further adding that sufficient $NaNO_3$ did not lead to gelation but only made **4a** aggregate and eventually precipitate; above the CGC, the **4a** solution turned into hydrogel quickly. Their gel states were confirmed by rheology studies, as discussed in the Supporting Information.

To understand the gelation process, transmission electron microscopy (TEM) and scanning electron microscopy (SEM) studies were performed. A dilute solution at 5.0 mg/mL was used to avoid severe aggregation on the TEM grid. Addition of 8 equiv of $NaNO_3$ leads to the aggregation of **4a**, confirmed by the SLS study. TEM images (Figure 3) on this sample showed

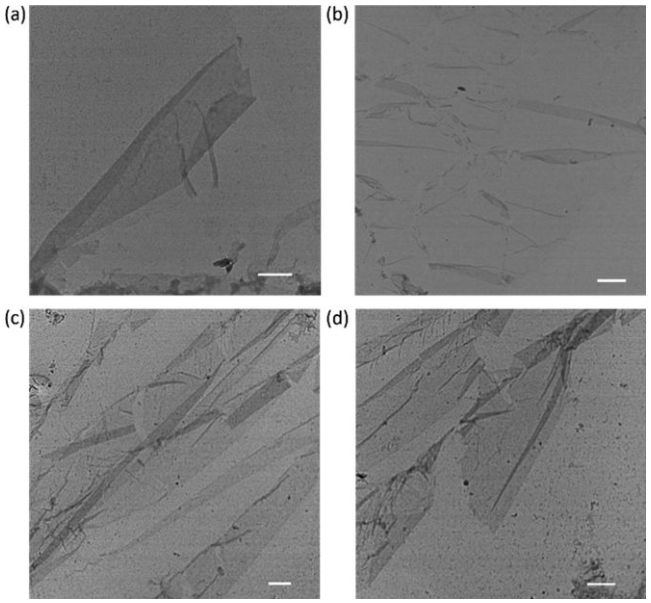


Figure 3. TEM images of 5 mg/mL **4a** solution with (a,b) 5 and (c,d) 8 equiv of $NaNO_3$. Scale bar: (a) 600 nm, (b) 2 μm, and (c,d) 1 μm.

hundreds of micrometer-sized 2D nanosheets. In addition, the SEM study (Figure 4) on the freeze-dried hydrogel sample

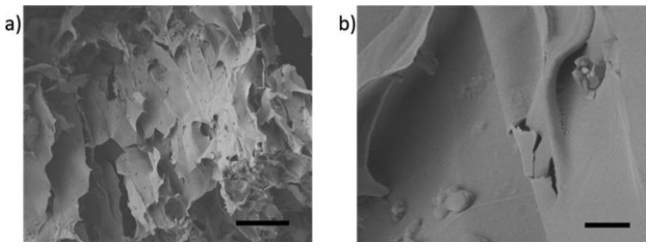


Figure 4. SEM images of the freeze-dried hydrogel from **4a**. Scale bar: (a) 100 μm, (b) 5 μm.

suggested 3D porous structures from 2D sheets, which were stacked together, with several hundred nanometers in thickness. The thick sheets dislocated from each other and were stacked together again to give 3D porous structures. However, similar MOC, **4b**, reported by Stang et al.,[58] formed a 2D lamellar structure but no gelation.

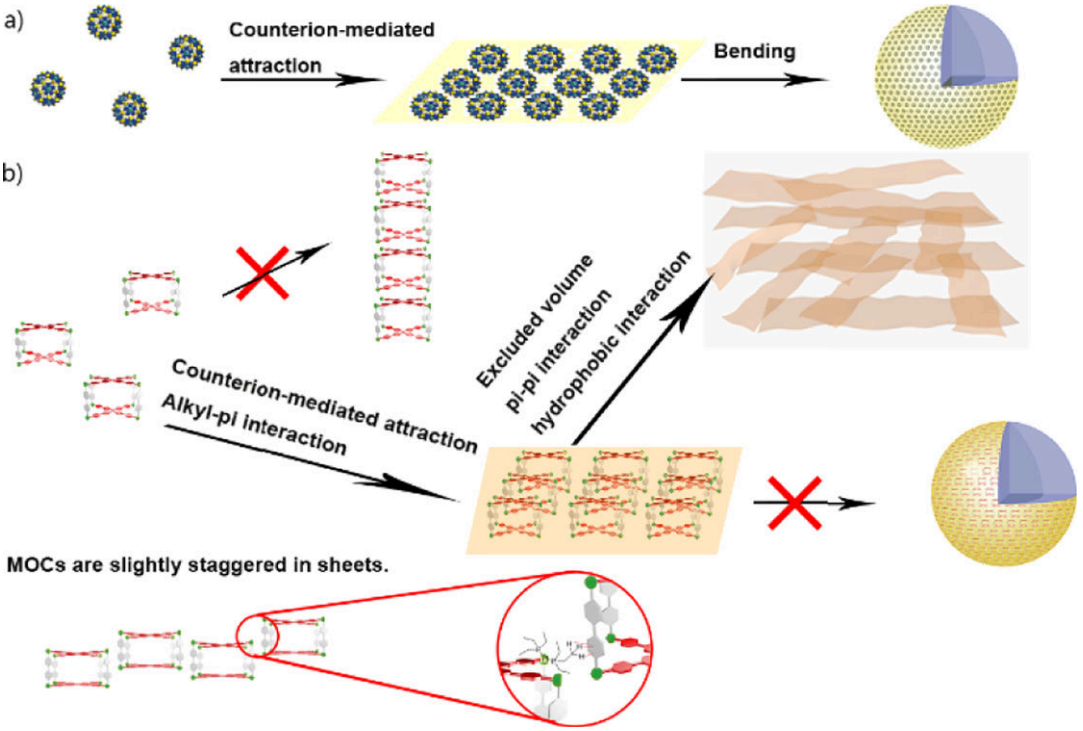
In this hydrogel system, there are only **4a**, $NaNO_3$, and water but no high-molecular-weight gelators such as polymers. Small molecules have been reported to construct polymeric structures and form gels through noncovalent interactions, such as metal−ligand coordination, hydrogen bonding, or hydrophobic interaction.[33] However, none of them seems to be the primary driving force in this study because (1) there is no chemical reaction and thus no dynamic coordination sites are available; (2) **4a** are neither ordinary hydrogen bonding donors nor acceptors; (3) 1D fiber structures are not observed, which should be the primary structures if hydrophobic interactions are the major driving forces for gelation because **4a** contains two hydrophobic **1a** on the opposite faces. In addition, electrostatic interaction often does not favor gelation because the electrostatic repulsion stabilizes the single molecules and the electrostatic attraction will promote aggregation.

TEM and SEM studies show the formation of nanosheets from **4a** in an aqueous solution, followed by the crosslinking/stacking of nanosheets into a 3D network, where gelation takes place. Previously, we demonstrated by experiments and simulations that the macroions with modest charge density can self-assemble into 2D single-layered structures, which eventually spontaneously bend into hollow spherical blackberry-type structures when the bending energy can be compensated by the increasing edge energy with the growing sheet size.[51] Here, MOCs still form single layers; however, with a cuboid-like structure, after the $\sigma-\pi$ interaction between **3** and **2a**, as well as the unique charge distribution, the resulting single layer cannot be bent easily because the process involves an obvious fracturing of the counterion-mediated attraction as well as $\sigma-\pi$ interaction and is therefore energetically unfavored. The $\sigma-\pi$ interaction between the alkyl groups and aromatic groups has been widely observed since 1952.[59] The weak attraction between the ethyl groups within **3** and the phenol rings within **2a**, confirmed by simulation, could further stabilize the existing large nanosheets. Consequently, instead of forming closed blackberry structures, **4a** stay as large nanosheets. Therefore, counteranion-mediated attraction among MOCs is expected to occur in the first stage. The associated NO_3^- ions will likely not stay around the electron-rich **1a**; instead, they are probably distributed near the cationic Pt corners and **2a** (electrostatic interaction) and act as bridges to link cages. This mechanism explains that the cages do not form 1-D fibers (requiring one preferred direction for interaction, i.e., **1a**) but 2-D nanosheets (Scheme 1b).

X-ray diffraction (XRD) measurements, determining the Pt−Pt distances, also support the counterion-mediated attraction model between MOCs. The freeze-dried sample from cage solution with nanosheets only showed one characteristic peak at the scattering angle of 11.3°, corresponding to a distance of 7.8 Å. The distance is too large for any intracage Pt−Pt distance (1.82, 1.52, or 1.21 Å) and can therefore only be assigned to the distance between adjacent cages. Also, it is too far for any hydrophobic[60,61] and $\pi-\pi$ interactions[62] or van der Waals forces,[60] suggesting that the structures are formed mainly based on counterion-mediated

https://dx.doi.org/10.1021/acsami.0c16366
ACS Appl. Mater. Interfaces 2020, 12, 56310−56318

Scheme 1. (a) Nanosheets and Blackberry Structures Formed by Polyoxometalate Macroions; (b) Proposed Self-Assembly Process from 4a in its aqueous Solution with the Addition of $NaNO_3$[a]



[a]Counterion-mediated attraction promotes the formation of nanosheets from **4a** which are stabilized by unique cage conformation, charge distribution, and $\sigma-\pi$ interaction. (Counterions are omitted for clearance.)

long-range electrostatic attraction. With $NaNO_3$ added, the solution turned into a gel and an intense peak at the scattering angle of 28.1° (correlated to a distance of 3.2 Å) appeared in addition to the original peak at 11.3°. Compared to the solution state, this peak is obtained because of the stacking of nanosheets and thus should be attributed to the intersheet distance (Figure 5). Because the surfaces of the sheets are composed of **1a** and the distance 3.2 Å is less than the maximum effective distance of hydrophobic/$\pi-\pi$ interactions (~5 Å), the nanosheets are likely to be stacked based on these interactions. This gelation process is likely to be similar to that of graphene oxide (GO), where the GO sheets form 3D porous networks based on the hydrophobic/$\pi-\pi$ interactions.

The importance of the additional electrolytes was further studied by adding different salts into the aqueous solutions of **4a** (15.0 mg/mL). The role of cations (acting as co-ions) was first investigated. Four types of nitrate salts, KNO_3, NH_4NO_3, $Co(NO_3)_2$, and $Ce(NO_3)_3$, were used to trigger the gelation of **4a**. All the nitrate salts showed similar results: all of them could trigger the gelation of **4a** and the critical salt concentrations (CSCs) are 8 equiv (in terms of NO_3^-), indicating that the cations did not affect the gelation process greatly, consistent with our expectation because the cationic MOCs strongly repel cations. Isothermal titration calorimetry (ITC) studies at a low cage concentration (0.1 mM) showed that NO_3^- anions did not strongly bind with **4a**, and the obtained thermodynamic parameters did not change with the type of cations.

The counterions are expected to be critical for the gelation process. Sodium salts with different anions were used to test this. From the gelation process, the effects of extra anions can be divided into two groups: (1) NO_3^-, I^-, PF_6^-, CF_3COO^-, $H_2PO_4^-$, ClO_4^-, and SO_4^{2-}, which can trigger the gelation; (2) F^-, Cl^-, Br^-, CH_3COO^-, HCO_3^-, SCN, and HPO_4^{2-}, which tend to precipitate **Cage 1** from the solution (Scheme 2). In group 1, the CSC values vary from low to high, the trend is as follows: $ClO_4^- \sim PF_6^- < I^- < CF_3COO^- \sim NO_3^- < SO_4^{2-} < H_2PO_4^-$.

It is interesting to note that the anionic valence is not the major factor affecting gelation capability because SO_4^{2-} is weaker than many monovalent anions. ITC titration curves at a low cage concentration (to avoid precipitation/aggregation) can be fitted by an independent model (Table S1), indicating that only one type of binding site on **4a** is available for counterions. The binding stoichiometry values were determined as 2 for most anions, which means two anions can bind to each **4a**, except 6 for PF_6^- and ClO_4^- and 8 for SCN^-. From the fitting results, PF_6^-, ClO_4^-, and I^- showed lower ΔG values (−17.8, −21.0, and −16.8 kJ/mol for I^-, ClO_4^-, and PF_6^-, respectively) during the binding process, indicating that they can easily bind with cages. This nicely explains that they can trigger gelation with less amounts and give a chance to further decrease the CGC when using these anions. The strong interactions between these anions and MOCs make it possible to obtain the gels with less amount of MOCs present.CF_3COO^- and NO_3^- anions show higher ΔG values (−13.0 kJ/mol for CF_3COO^- and −16.5 kJ/mol for NO_3^-), corresponding to the observation that larger amounts are needed for gelation. The observations here suggest that instead of valence, the hydration shell thickness of anions (Table S2) is more important for gelation because anions with a thick hydration shell showed weak binding affinity to **4a**.[63] There is a large enthalpy loss when the ions with a thicker hydration shell are dehydrated during the ion-pair formation process, which shows weaker binding affinity and requires a larger amount of

https://dx.doi.org/10.1021/acsami.0c16366
ACS Appl. Mater. Interfaces 2020, 12, 56310−56318

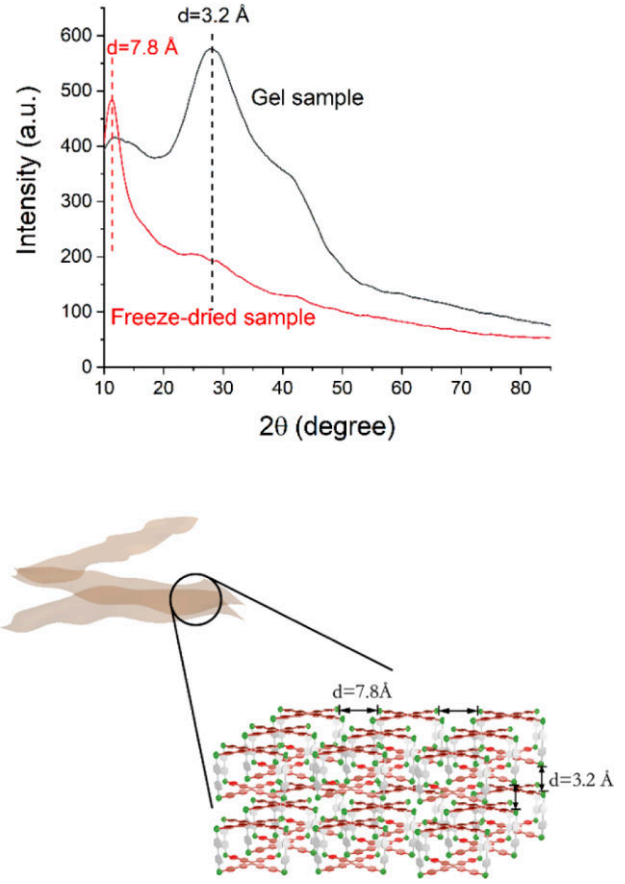
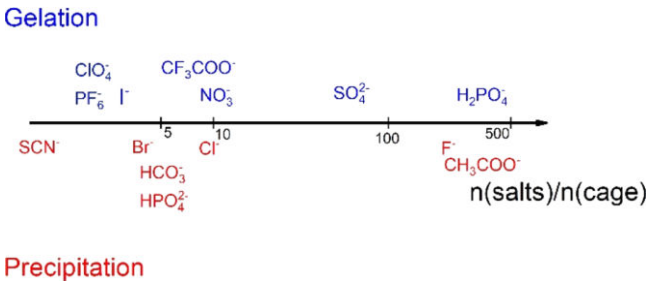


Figure 5. XRD patterns of the freeze-dried **4a** sample and gel sample. (MOCs are slightly staggered in sheets, which are not shown here.)

Scheme 2. Gelation or Precipitation Triggered by Various Anions at Different Salt/Cage Ratios



salt to trigger gelation. Overall, this trend correlates well with the inverse Hofmeister series where "salt-out" anions are easier to trigger the gelation and CGC values for "salt-in" anions are higher. The sequence is opposite to the Hofmeister series, probably because macrocationic cages are used instead of negatively charged proteins.[64,65]

The other group of anions can only make **4a** precipitate out. The amounts of these anions to precipitate **4a** have the trend as follows: $F^- \sim CH_3COO^- > Cl^- > Br^- \sim HCO_3^- \sim HPO_4^{2-} > SCN^-$. It is also consistent with the inverse Hofmeister series, where anions with thicker hydration shells showed weak ability to precipitate **4a**. The binding affinities were also confirmed by the ITC study (Table S1). The reason for these anions to precipitate the cages rather than turning the cage solution into a gel probably lies in either the smaller Van der Waals radius (Br^-, Cl^-, and F^-) or more specific interaction with the cages.[66−68]

Interestingly, if the length of the dicarboxylic ligands was shortened from 1.52 to 0.70 Å, **4b** cannot undergo the gelation process, even with a large amount of salts, only precipitates can be observed. This indicates that long edges in MOCs are important for the gelation as it may provide stronger counterion-mediated attraction and more chance for $\sigma-\pi$ interaction to stabilize the nanosheets. In addition, the longer edges make the bending of the nanosheet more difficult, which helps to improve the stability of the nanosheets in solution. Moreover, another similar MOC, **4c**, shows no ordered self-assembled structure and only precipitates as well, which suggests that the $\sigma-\pi$ interaction between the edges and corners is significant for stabilizing the nanosheets.

To better understand the self-assembly of the above molecular cages, we have performed atomistic molecular dynamics (MD) simulations of separate **4a**, **4b**, and **4c** cages (six in each system) in solutions with 10 equiv of $NaNO_3$ and neutralized by additional NO_3^- counterions. Figure 6 shows the top and side views of the final supramolecular configurations for **4a**, **4b**, and **4c** as well as atomic density isosurface of neighboring cages and NO_3^- ions around a specific cage. **4a** (Figure 6a−c) forms a 2D unimolecular network through $\sigma-\pi$ noncovalent bonds from its corner to the edge of the neighboring cages. Because **4a** has two aromatic groups on the edges, it can easily form a "double $\sigma-\pi$ noncovalent bond", which strengthens this interaction. The atomic density isosurface of neighboring cages shows that the neighboring cages bind primarily through the edge aromatic groups and corner ligands but not the face aromatic groups. This steric arrangement facilitates a "lock and key" binding that propagates into a 2D network because propagation through the faces does not occur.

There is only one aromatic group on each edge in **4b**, so the "double $\sigma-\pi$ noncovalent bond" is not structurally very likely. Therefore, the alkyl groups of the ligands at the corners interact weaker with the edges and some of those ligands interact with the faces of a neighboring cage (Figure 6g). As a result, the supramolecular cluster of **4b** is less ordered than the supramolecular cluster of **4a** (Figure 6e,f). After the supramolecular structure is formed, it undergoes internal conformational changes. A 3D disordered supramolecular structure of **4b** forms because the cages can bind through the faces as well as the ligands, unlike the cages of **4a**.

The formation of "double $\sigma-\pi$ noncovalent bonds" is structurally possible in **4c**, giving different supramolecular structures than **4a** or **4b** (Figure 6i,j). Rather than forming a 2D network or a highly disordered 3D cluster, **4c** cages form 1D chains. This is because the $\sigma-\pi$ interaction occurs through the faces rather than through the edges (Figure 6i). In **4c**, the functional groups on faces and edges, which bind to the Pt center, are reversed from those of **4a**, that is, the carboxyl groups are on the faces and the pyridine groups are on the edges. The **4c** cages bind through the faces rather than through the edges. This causes a 1D chain growth rather than the formation of a broader 2D network observed in **4a**. It seems that the corner ligands in **3** have a preference to form $\sigma-\pi$ interactions with aromatic groups adjacent to carboxyl acids rather than pyridine groups.

The carboxyl groups in **1b**, **2a**, and **2b** tend to withdraw electrons from the neighboring aromatic groups, whereas the pyridine groups in **1a** and **2c** add electrons within the adjacent

https://dx.doi.org/10.1021/acsami.0c16366
ACS Appl. Mater. Interfaces 2020, 12, 56310−56318

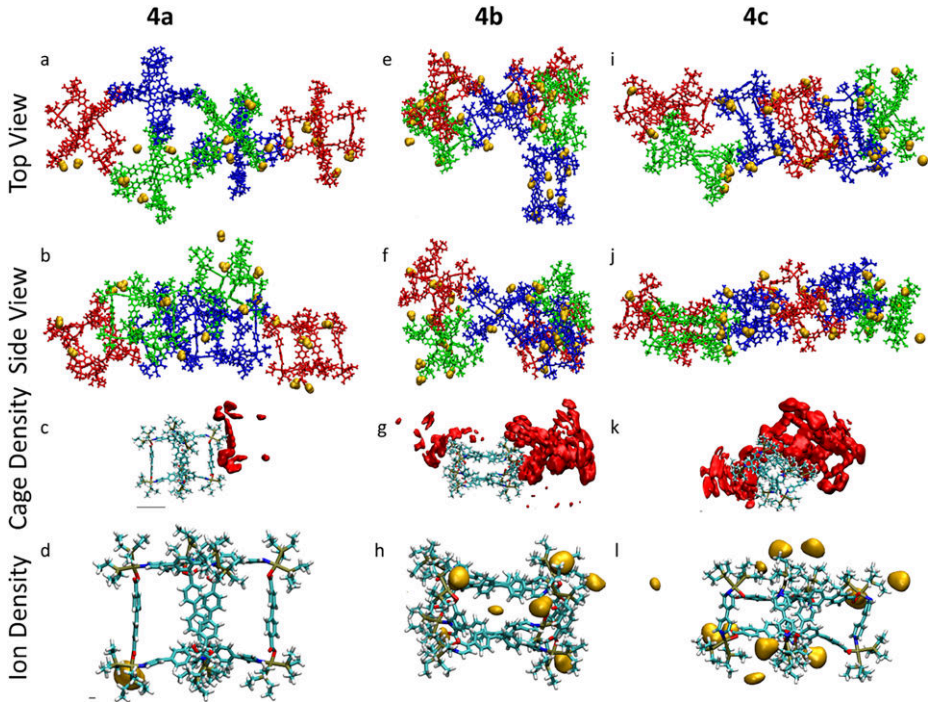


Figure 6. (a,b) Top and side views of the supramolecular structure of **4a** and neighboring NO_3^- ions after 205 ns long simulations. (c) Atomic density isosurface of neighboring cages around one cage with the **4a** structure. (d) Atomic density isosurface of NO_3^- ions around one cage with the **4a** structure. (e,f) Top and side views of a supramolecular structure of **4b** and neighboring NO_3^- ions after 259 ns. (g) Atomic density isosurface of neighboring cages around one cage with the **4b** structure. (h) Atomic density isosurface of NO_3^- ions around one cage with the **4b** structure. (i,j) Top and side views of the supramolecular structure of **4c** and neighboring NO_3^- ions after 340 ns. (k) Atomic density isosurface of neighboring cages around one cage with the **4c** structure. (l) Atomic density isosurface of NO_3^- ions around one cage with the **4c** structure. Scale bar in inset c represents 1 nm for insets (a–c,e–g,i–k). Scale bar in inset l represents 1 Å for insets (d,h,l).

aromatic groups. The $\sigma-\pi$ interactions would more likely occur with aromatic groups that have lower electron densities, that is, those adjacent to carboxyl groups. Therefore, **4a** has an electronic and steric structure that fits the formation of a 2D network, which is not possible in **4b**, due to steric effects. **4c** has a different electronic structure in the faces and sides, leading to different supramolecular structures. More cages with different corners, yet the same edges and faces as **4a** and **4b**, have been simulated and discussed in the Supporting Information.

Counterion-mediated attraction among the cages is important for the self-assembly processes because each cage has a net charge of +8e. In all radial distribution functions of the N atom in the NO_3^- with respect to the Pt atom, the most intense peaks occurred at $r \sim 3.5$ Å (refer to Supporting Information). Integration of the peak yields 1, which means that there is a high probability an NO_3^- ion located close to the charged Pt atom, which screens the charge of the Pt atom. NO_3^- ions were all outside the cages and close to the Pt atoms according to our atomic density isosurfaces (Figure 6d,h,l). This enables bridging between the highly charged cages. In addition, the NO_3^- ions had a tendency to be closer to the faces, rather than the sides regardless of the electronic structure of the faces. This indicates that steric factors influence the position of counterions more than the electronic structure of the cages. The counterion-mediated attraction among cages was indicated by the Pt–Pt distance, determined to be 7.8 Å by XRD, and Pt–NO_3^- distance, 3.5 Å obtained by simulation. During the self-assembly process, cages come close to each other because of the counterion-mediated attraction, forming 2D nanosheets, stabilized by $\sigma-\pi$ interaction and the large excluded volume leads to gelation with the assistance of hydrophobic/partial $\pi-\pi$ interactions.

CONCLUSIONS

In summary, we report a physical hydrogel formation process from a 2 nm sized cuboid-like MOC at low cage concentrations based on counterion-mediated attraction. With the addition of extra salts, the cages will first form large 2-D nanosheets in aqueous solution based on counterion-mediated attraction, which are stabilized by unique cage conformation, charge density, as well as $\sigma-\pi$ interaction, confirmed by the simulation results; the resulting hydrophobic sheets behave similar to GO and form a porous network, where the hydrophobic sheets were stacked because of hydrophobic/$\pi-\pi$ interactions. The hydrogel presents typical weak physical gel properties and can undergo temperature-controlled sol–gel transitions. Different counteranions show different effects on the gel formation, mostly controlled by their hydrated sizes instead of valence, while the effect of co-ions is negligible. This work elaborates the gelation process from low-molecular-weight gelators with electrostatic interaction dominated, which distinguishes itself from traditional gel systems, for instance, fiber entanglements.

ASSOCIATED CONTENT

Supporting Information

The Supporting Information is available free of charge at https://pubs.acs.org/doi/10.1021/acsami.0c16366.

^{1}H NMR, DLS, TEM, ITC, and all-atom simulation (PDF)

https://dx.doi.org/10.1021/acsami.0c16366
ACS Appl. Mater. Interfaces 2020, 12, 56310–56318

AUTHOR INFORMATION

Corresponding Authors

Hui Li − *Center for Nanophase Materials Sciences, Oak Ridge Nation Laboratory, Oak Ridge, Tennessee 37831, United States;* orcid.org/0000-0002-6964-9962; Email: lih2@ornl.gov

Petr Král − *Department of Chemistry, Physics, Biopharmaceutical Sciences, and Chemical Engineering, University of Illinois at Chicago, Chicago, Illinois 60607, United States;* orcid.org/0000-0003-2992-9027; Email: pkral@uic.edu

Tianbo Liu − *The School of Polymer Science and Polymer Engineering, The University of Akron, Akron, Ohio 44325-3909, United States;* orcid.org/0000-0002-8181-1790; Email: tliu@uakron.edu

Authors

Yuqing Yang − *The School of Polymer Science and Polymer Engineering, The University of Akron, Akron, Ohio 44325-3909, United States;* orcid.org/0000-0002-5407-5740

Pavel Rehak − *Department of Chemistry, University of Illinois at Chicago, Chicago, Illinois 60607, United States*

Ting-Zheng Xie − *Environmental Research at Greater Bay Area, Key Laboratory for Water Quality and Conservation of the Pearl River Delta, Ministry of Education, Guangzhou Key Laboratory for Clean Energy and Materials, Guangzhou University, Guangzhou 510006, China;* orcid.org/0000-0001-6717-7642

Yi Feng − *The School of Polymer Science and Polymer Engineering, The University of Akron, Akron, Ohio 44325-3909, United States*

Xinyu Sun − *The School of Polymer Science and Polymer Engineering, The University of Akron, Akron, Ohio 44325-3909, United States;* orcid.org/0000-0003-4353-1832

Jiahui Chen − *The School of Polymer Science and Polymer Engineering, The University of Akron, Akron, Ohio 44325-3909, United States;* orcid.org/0000-0002-3861-146X

Complete contact information is available at: https://pubs.acs.org/10.1021/acsami.0c16366

Notes

The authors declare no competing financial interest.

ACKNOWLEDGMENTS

T.L. acknowledges support from the National Science Foundation (CHE1904397), The University of Akron and Dr. Andrew Knoll for the help on XRD measurement, Rodger Dilla and Dr. Matthew Becker for their help on freeze-drying. We also thank Dr. Mrinal Kanti Bera at NSF's ChemMatCARS for helping on the SAXS measurements. ChemMatCARS Sector 15 is supported by the Divisions of Chemistry (CHE) and Materials Research (DMR), National Science Foundation, under grant number NSF/CHE-1834750. Use of the Advanced Photon Source, an Office of Science User Facility operated for the U.S. Department of Energy (DOE) Office of Science by Argonne National Laboratory, was supported by the U.S. DOE under contract no. DE-AC02-06CH11357

REFERENCES

(1) Jacobson, A. J. Colloidal Dispersions of Compounds with Layer and Chain Structures. *Mater. Sci. Forum* **1994**, *152*−*153*, 1−12.

(2) Zhang, L.; Chen, D.; Jiao, X. Monoclinic Structured BiVO4 Nanosheets: Hydrothermal Preparation, Formation Mechanism, and Coloristic and Photocatalytic Properties. *J. Phys. Chem. B* **2006**, *110*, 2668−2673.

(3) Penn, R. L.; Banfield, J. F. Imperfect Oriented Attachment: Dislocation Generation in Defect-Free Nanocrystals. *Science* **1998**, *281*, 969.

(4) Banfield, J. F.; Welch, S. A.; Zhang, H.; Ebert, T. T.; Penn, R. L. Aggregation-Based Crystal Growth and Microstructure Development in Natural Iron Oxyhydroxide Biomineralization Products. *Science* **2000**, *289*, 751.

(5) Wang, C.; Du, G.; StÅhl, K.; Huang, H.; Zhong, Y.; Jiang, J. Z. Ultrathin SnO2 Nanosheets: Oriented Attachment Mechanism, Nonstoichiometric Defects, and Enhanced Lithium-Ion Battery Performances. *J. Phys. Chem. C* **2012**, *116*, 4000−4011.

(6) Bhattarai, N.; Gunn, J.; Zhang, M. Chitosan-Based Hydrogels for Controlled, Localized Drug Delivery. *Adv. Drug Deliv. Rev.* **2010**, *62*, 83−99.

(7) Buenger, D.; Topuz, F.; Groll, J. Hydrogels in Sensing Applications. *Prog. Polym. Sci.* **2012**, *37*, 1678−1719.

(8) Lee, K. Y.; Mooney, D. J. Hydrogels for tissue engeneering. *Chem. Rev.* **2001**, *101*, 1869−1880.

(9) Parente, M. E.; Ochoa Andrade, A.; Ares, G.; Russo, F.; Jiménez-Kairuz, Á. Bioadhesive Hydrogels for Cosmetic Applications. *Int. J. Cosmet. Sci.* **2015**, *37*, 511−518.

(10) Farris, S.; Schaich, K. M.; Liu, L.; Piergiovanni, L.; Yam, K. L. Development of Polyion-Complex Hydrogels as an Alternative Approach for the Production of Bio-Based Polymers for Food Packaging Applications: a Review. *Trends Food Sci. Technol.* **2009**, *20*, 316−332.

(11) Tongwa, P.; Bai, B. Degradable Nanocomposite Preformed Particle Gel for Chemical Enhanced Oil Recovery Applications. *J. Petrol. Sci. Eng.* **2014**, *124*, 35−45.

(12) Yan, X.; Xu, D.; Chi, X.; Chen, J.; Dong, S.; Ding, X.; Yu, Y.; Huang, F. A Multiresponsive, Shape-Persistent, and Elastic Supramolecular Polymer Network Gel Constructed by Orthogonal Self-Assembly. *Adv. Mater.* **2012**, *24*, 362−369.

(13) Zheng, W.; Chen, L.-J.; Yang, G.; Sun, B.; Wang, X.; Jiang, B.; Yin, G.-Q.; Zhang, L.; Li, X.; Liu, M.; Chen, G.; Yang, H.-B. Construction of Smart Supramolecular Polymeric Hydrogels Cross-linked by Discrete Organoplatinum(II) Metallacycles via Post-Assembly Polymerization. *J. Am. Chem. Soc.* **2016**, *138*, 4927−4937.

(14) Liu, Y.; Shi, B.; Wang, H.; Shangguan, L.; Li, Z.; Zhang, M.; Huang, F. Construction of Metallacage-Cored Supramolecular Gel by Hierarchical Self-Assembly of Metal Coordination and Pillar[5]arene-Based Host−Guest Recognition. *Macromol. Rapid Commun.* **2018**, *39*, 1800655.

(15) Wei, S.-C.; Pan, M.; Fan, Y.-Z.; Liu, H.; Zhang, J.; Su, C.-Y. Creating Coordination-Based Cavities in a Multiresponsive Supramolecular Gel. *Chem.: Eur. J.* **2015**, *21*, 7418−7427.

(16) Li, Z.-Y.; Zhang, Y.; Zhang, C.-W.; Chen, L.-J.; Wang, C.; Tan, H.; Yu, Y.; Li, X.; Yang, H.-B. Cross-Linked Supramolecular Polymer Gels Constructed from Discrete Multi-pillar[5]arene Metallacycles and Their Multiple Stimuli-Responsive Behavior. *J. Am. Chem. Soc.* **2014**, *136*, 8577−8589.

(17) Yan, X.; Cook, T. R.; Pollock, J. B.; Wei, P.; Zhang, Y.; Yu, Y.; Huang, F.; Stang, P. J. Responsive Supramolecular Polymer Metallogel Constructed by Orthogonal Coordination-Driven Self-Assembly and Host/Guest Interactions. *J. Am. Chem. Soc.* **2014**, *136*, 4460−4463.

(18) Feng, J.; Zeng, L.; Chen, K.; Fang, H.; Zhang, J.; Chi, Z.; Su, C.-Y. Gelation of Luminescent Supramolecular Cages and Transformation to Crystals with Trace-Doped-Enhancement Luminescence. *Langmuir* **2016**, *32*, 12184−12189.

(19) Zhou, Z.; Yan, X.; Cook, T. R.; Saha, M. L.; Stang, P. J. Engineering Functionalization in a Supramolecular Polymer: Hierarchical Self-Organization of Triply Orthogonal Non-covalent Interactions on a Supramolecular Coordination Complex Platform. *J. Am. Chem. Soc.* **2016**, *138*, 806−809.

(20) Wu, N.-W.; Chen, L.-J.; Wang, C.; Ren, Y.-Y.; Li, X.; Xu, L.; Yang, H.-B. Hierarchical Self-Assembly of a Discrete Hexagonal

Metallacycle into the Ordered Nanofibers and Stimuli-Responsive Supramolecular Gels. *Chem. Commun.* **2014**, *50*, 4231−4233.
(21) Shi, Y.; Wang, M.; Ma, C.; Wang, Y.; Li, X.; Yu, G. A Conductive Self-Healing Hybrid Gel Enabled by Metal−Ligand Supramolecule and Nanostructured Conductive Polymer. *Nano Lett.* **2015**, *15*, 6276−6281.
(22) Zhang, Y.; Zhou, Q.-F.; Huo, G.-F.; Yin, G.-Q.; Zhao, X.-L.; Jiang, B.; Tan, H.; Li, X.; Yang, H.-B. Hierarchical Self-Assembly of an Alkynylplatinum(ll) Bzimpy-Functionalized Metallacage via Pt···Pt and $\pi-\pi$ Interactions. *Inorg. Chem.* **2018**, *57*, 3516−3520.
(23) Ganta, S.; Chand, D. K. Multi-Stimuli-Responsive Metallogel Molded from a Pd2L4-Type Coordination Cage: Selective Removal of Anionic Dyes. *Inorg. Chem.* **2018**, *57*, 3634−3645.
(24) Sun, B.; Wang, M.; Lou, Z.; Huang, M.; Xu, C.; Li, X.; Chen, L.-J.; Yu, Y.; Davis, G. L.; Xu, B.; Yang, H.-B.; Li, X. From Ring-in-Ring to Sphere-in-Sphere: Self-Assembly of Discrete 2D and 3D Architectures with Increasing Stability. *J. Am. Chem. Soc.* **2015**, *137*, 1556−1564.
(25) Jiang, B.; Zhang, J.; Zheng, W.; Chen, L.-J.; Yin, G.-Q.; Wang, Y.-X.; Sun, B.; Li, X.; Yang, H.-B. Construction of Alkynylplatinum-(II) Bzimpy-Functionalized Metallacycles and Their Hierarchical Self-Assembly Behavior in Solution Promoted by Pt···Pt and $\pi-\pi$ Interactions. *Chem.: Eur. J.* **2016**, *22*, 14664−14671.
(26) Sun, Y.; Li, S.; Zhou, Z.; Saha, M. L.; Datta, S.; Zhang, M.; Yan, X.; Tian, D.; Wang, H.; Wang, L.; Li, X.; Liu, M.; Li, H.; Stang, P. J. Alanine-Based Chiral Metallogels via Supramolecular Coordination Complex Platforms: Metallogelation Induced Chirality Transfer. *J. Am. Chem. Soc.* **2018**, *140*, 3257−3263.
(27) Lu, C.; Zhang, M.; Tang, D.; Yan, X.; Zhang, Z.; Zhou, Z.; Song, B.; Wang, H.; Li, X.; Yin, S.; Sepehrpour, H.; Stang, P. J. Fluorescent Metallacage-Core Supramolecular Polymer Gel Formed by Orthogonal Metal Coordination and Host−Guest Interactions. *J. Am. Chem. Soc.* **2018**, *140*, 7674−7680.
(28) Ren, Y.-Y.; Xu, Z.; Li, G.; Huang, J.; Fan, X.; Xu, L. Hierarchical Self-Assembly of a Fluorescence Emission-Enhanced Organogelator and its Multiple Stimuli-Responsive Behaviors. *Dalton Trans.* **2017**, *46*, 333−337.
(29) Moura, M. J.; Faneca, H.; Lima, M. P.; Gil, M. H.; Figueiredo, M. M. In Situ Forming Chitosan Hydrogels Prepared via Ionic/Covalent Co-Cross-Linking. *Biomacromolecules* **2011**, *12*, 3275−3284.
(30) Dash, M.; Chiellini, F.; Ottenbrite, R. M.; Chiellini, E. Chitosan—A versatile semi-synthetic polymer in biomedical applications. *Prog. Polym. Sci.* **2011**, *36*, 981−1014.
(31) Kim, G.; Kim, N.; Kim, D.; Kwon, J.; Min, B.-H. An electrostatically crosslinked chitosan hydrogel as a drug carrier. *Molecules* **2012**, *17*, 13704−13711.
(32) Hu, Y.; Zhang, Z.; Li, Y.; Ding, X.; Li, D.; Shen, C.; Xu, F.-J. Dual-Crosslinked Amorphous Polysaccharide Hydrogels Based on Chitosan/Alginate for Wound Healing Applications. *Macromol. Rapid Commun.* **2018**, *39*, 1800069.
(33) Tam, A. Y.-Y.; Yam, V. W.-W. Recent Advances in Metallogels. *Chem. Soc. Rev.* **2013**, *42*, 1540−1567.
(34) Lehn, J. M.; Sanders, J. Book review: chemistry beyond the molecule: supramolecular chemistry. Concepts and perspectives. *Angew. Chem. Int. Ed.* **1995**, *34*, 2563.
(35) Chakrabarty, R.; Mukherjee, P. S.; Stang, P. J. Supramolecular Coordination: Self-Assembly of Finite Two- and Three-Dimensional Ensembles. *Chem. Rev.* **2011**, *111*, 6810−6918.
(36) Fujita, M.; Tominaga, M.; Hori, A.; Therrien, B. Coordination Assemblies from a Pd(II)-Cornered Square Complex. *Acc. Chem. Res.* **2005**, *38*, 369−378.
(37) Fujita, M. Metal-Directed Self-Assembly of Two- and Three-Dimensional Synthetic Receptors. *Chem. Soc. Rev.* **1998**, *27*, 417−425.
(38) Leininger, S.; Olenyuk, B.; Stang, P. J. Self-Assembly of Discrete Cyclic Nanostructures Mediated by Transition Metals. *Chem. Rev.* **2000**, *100*, 853−908.
(39) Schultz, A.; Li, X.; Moorefield, C. N.; Wesdemiotis, C.; Newkome, G. R. Self-Assembly and Characterization of 3D Metallamacrocycles: A Study of Supramolecular Constitutional Isomers. *Eur. J. Inorg. Chem.* **2013**, *2013*, 2492−2497.
(40) Newkome, G. R.; Moorefield, C. N. From 1 → 3 Dendritic Designs to Fractal Supramacromolecular Constructs: Understanding the Pathway to the Sierpiński gasket. *Chem. Soc. Rev.* **2015**, *44*, 3954−3967.
(41) Smulders, M. M. J.; Riddell, I. A.; Browne, C.; Nitschke, J. R. Building on Architectural Principles for Three-Dimensional Metallosupramolecular Construction. *Chem. Soc. Rev.* **2013**, *42*, 1728−1754.
(42) Riddell, I. A.; Smulders, M. M. J.; Clegg, J. K.; Hristova, Y. R.; Breiner, B.; Thoburn, J. D.; Nitschke, J. R. Anion-induced reconstitution of a self-assembling system to express a chloride-binding Co10L15 pentagonal prism. *Nat. Chem.* **2012**, *4*, 751−756.
(43) Machan, C. W.; Adelhardt, M.; Sarjeant, A. A.; Stern, C. L.; Sutter, J.; Meyer, K.; Mirkin, C. A. One-Pot Synthesis of an Fe(II) Bis-Terpyridine Complex with Allosterically Regulated Electronic Properties. *J. Am. Chem. Soc.* **2012**, *134*, 16921−16924.
(44) Kennedy, R. D.; Machan, C. W.; McGuirk, C. M.; Rosen, M. S.; Stern, C. L.; Sarjeant, A. A.; Mirkin, C. A. General Strategy for the Synthesis of Rigid Weak-Link Approach Platinum(II) Complexes: Tweezers, Triple-Layer Complexes, and Macrocycles. *Inorg. Chem.* **2013**, *52*, 5876−5888.
(45) Caulder, D. L.; Raymond, K. N. Supermolecules by Design. *Acc. Chem. Res.* **1999**, *32*, 975−982.
(46) Liu, D.; Liu, H.; Song, B.; Chen, M.; Huang, J.; Wang, J.; Yang, X.; Sun, W.; Li, X.; Wang, P. Terpyridine-Based Metallo-Organic Cages and Supramolecular Gelation by Coordination-Driven Self-Assembly and Host−Guest Interaction. *Dalton Trans.* **2018**, *47*, 14227−14232.
(47) Sciortino, F.; Buldyrev, S. V.; De Michele, C.; Foffi, G.; Ghofraniha, N.; La Nave, E.; Moreno, A.; Mossa, S.; Saika-Voivod, I.; Tartaglia, P.; Zaccarelli, E. Routes to colloidal gel formation. *Comput. Phys. Commun.* **2005**, *169*, 166−171.
(48) Deng, N.-J.; Luo, Y.-Z.; Tanodekaew, S.; Bingham, N.; Attwood, D.; Booth, C. Gelation of micellar solutions of diblock-copoly (oxyethylene/oxybutylene) in aqueous K2SO4. An investigation of excluded volume effects. *J. Polym. Sci., Part B: Polym. Phys.* **1995**, *33*, 1085−1096.
(49) Kapnistos, M.; Vlassopoulos, D.; Fytas, G.; Mortensen, K.; Fleischer, G.; Roovers, J. Reversible Thermal Gelation in Soft Spheres. *Phys. Rev. Lett.* **2000**, *85*, 4072−4075.
(50) Sutar, P.; Suresh, V. M.; Jayaramulu, K.; Hazra, A.; Maji, T. K. Binder Driven Self-Assembly of Metal-Organic Cubes Towards Functional Hydrogels. *Nat. Commun.* **2018**, *9*, 3587.
(51) Yin, P.; Li, D.; Liu, T. Solution behaviors and self-assembly of polyoxometalates as models of macroions and amphiphilic polyoxometalate−organic hybrids as novel surfactants. *Chem. Soc. Rev.* **2012**, *41*, 7368−7383.
(52) Yang, M.; Chan, H.; Zhao, G.; Bahng, J. H.; Zhang, P.; Král, P.; Kotov, N. A. Self-assembly of nanoparticles into biomimetic capsid-like nanoshells. *Nat. Chem.* **2017**, *9*, 287−294.
(53) Zhang, M.; Saha, M. L.; Wang, M.; Zhou, Z.; Song, B.; Lu, C.; Yan, X.; Li, X.; Huang, F.; Yin, S.; Stang, P. J. Multicomponent Platinum(II) Cages with Tunable Emission and Amino Acid Sensing. *J. Am. Chem. Soc.* **2017**, *139*, 5067−5074.
(54) Li, H.; Xie, T.-Z.; Liang, Z.; Dahal, D.; Shen, Y.; Sun, X.; Yang, Y.; Pang, Y.; Liu, T. Conformational change due to intramolecular hydrophobic interaction leads to large blue-shifted emission from single molecular cage solutions. *Chem. Commun.* **2019**, *55*, 330−333.
(55) Li, D.; Zhou, W.; Landskron, K.; Sato, S.; Kiely, C. J.; Fujita, M.; Liu, T. Viral-Capsid-Type Vesicle-Like Structures Assembled from M12L24 Metal−Organic Hybrid Nanocages. *Angew. Chem., Int. Ed.* **2011**, *50*, 5182−5187.
(56) Raee, E.; Li, H.; Sun, X.; Ustriyana, P.; Luo, J.; Chen, J.; Sahai, N.; Liu, T. Strong Enantiomeric Preference on the Macroion−Counterion Interaction Induced by Weakly Associated Chiral Counterions. *J. Phys. Chem. B* **2020**, *124*, 9958−9966.

https://dx.doi.org/10.1021/acsami.0c16366
ACS Appl. Mater. Interfaces 2020, 12, 56310−56318

(57) Pigga, J. M.; Teprovich, J. A.; Flowers, R. A.; Antonio, M. R.; Liu, T. Selective Monovalent Cation Association and Exchange around Keplerate Polyoxometalate Macroanions in Dilute Aqueous Solutions. *Langmuir* **2010**, *26*, 9449−9456.
(58) Sun, Y.; Zhang, F.; Jiang, S.; Wang, Z.; Ni, R.; Wang, H.; Zhou, W.; Li, X.; Stang, P. J. Assembly of Metallacages into Soft Suprastructures with Dimensions of up to Micrometers and the Formation of Composite Materials. *J. Am. Chem. Soc.* **2018**, *140*, 17297−17307.
(59) Nishio, M.; Hirota, M.; Umezawa, Y. *The CH/π Interaction: Evidence, Nature, and Consequences*; John Wiley & Sons, 1998; Vol. *21*.
(60) Israelachvili, J. N. *Intermolecular and Surface Forces*; Academic Press, 2015.
(61) Ashbaugh, H. S.; Pratt, L. R. Colloquium: Scaled Particle Theory and The Length Scales of Hydrophobicity. *Rev. Mod. Phys.* **2006**, *78*, 159−178.
(62) Janiak, C. A Critical Account on π−π Stacking in Metal Complexes with Aromatic Nitrogen-Containing Ligands. *J. Chem. Soc., Dalton Trans.* **2000**, *21*, 3885−3896.
(63) He, J.; Li, H.; Yang, P.; Haso, F.; Wu, J.; Li, T.; Kortz, U.; Liu, T. Tuning of Polyoxopalladate Macroanionic Hydration Shell via Countercation Interaction. *Chem. Eur. J.* **2018**, *24*, 3052−3057.
(64) Paterová, J.; Rembert, K. B.; Heyda, J.; Kurra, Y.; Okur, H. I.; Liu, W. R.; Hilty, C.; Cremer, P. S.; Jungwirth, P. Reversal of the Hofmeister Series: Specific Ion Effects on Peptides. *J. Phys. Chem. B* **2013**, *117*, 8150−8158.
(65) Zhang, Y.; Cremer, P. S. The inverse and direct Hofmeister series for lysozyme. *Proc. Natl. Acad. Sci. U.S.A.* **2009**, *106*, 15249.
(66) Lee, C.; Yang, W.; Parr, R. G. Local Softness and Chemical Reactivity in the Molecules CO, SCN− and H2CO. *J. Mol. Struct.: THEOCHEM* **1988**, *163*, 305−313.
(67) Bowman-James, K.; Bianchi, A.; García-España, E. *Anion Coordination Chemistry*; John Wiley & Sons, 2012.
(68) Zhang, T.; Zhang, G.-L.; Yan, Q.-Q.; Zhou, L.-P.; Cai, L.-X.; Guo, X.-Q.; Sun, Q.-F. Self-Assembly of a Tetraphenylethylene-Based Capsule Showing Both Aggregation- and Encapsulation-Induced Emission Properties. *Inorg. Chem.* **2018**, *57*, 3596−3601.

https://dx.doi.org/10.1021/acsami.0c16366
ACS Appl. Mater. Interfaces 2020, 12, 56310−56318